

# Moment Approach for Determining the Orbital Elements of an Astrometric Binary with Low Signal-to-noise Ratio

Hirofumi IWAMA, Hideki ASADA, Kei YAMADA

*Faculty of Science and Technology, Hirosaki University, Hirosaki, Aomori 036-8561*

*asada@phys.hirosaki-u.ac.jp*

(Received ; accepted )

## Abstract

A moment approach for orbit determinations of an astrometric binary with low signal-to-noise ratio from astrometric observations alone is proposed, especially aiming at a close binary system with a short orbital period such as Cyg-X1 and also at a star wobbled by planets. As an exact solution to the nonlinearly coupled equation system, the orbital elements are written in terms of the second and third moments of projected positions that are measured by astrometry. This may give a possible estimation of the true orbit.

**Key words:** astrometry — celestial mechanics — binaries: close — methods: analytical

## 1. Introduction

Space astrometry missions such as Gaia and JASMINE are expected to reach a few micro arcseconds (Mignard 2004 ; Perryman 2004 ; Gouda et al. 2007 ). Moreover, high-accuracy VLBI is also available.

For visual binaries, formulations for orbit determinations have been well developed since the nineteenth century (Thiele 1883 ; Binnendijk 1960 ; Aitken 1964 ; Danby 1988 ; Roy 1988 ). At present, numerical methods are successfully used (Eichhorn and Xu 1990 ; Catovic and Olevic 1992 ; Olevic and Cvetkovic 2004 ). Furthermore, an analytic solution for an astrometric binary, where one object can be observed and the other such as black holes and neutron stars is unseen, has been found (Asada et al. 2004 ; Asada 2008 ). The solution requires that sufficiently accurate measurements of the position of a star (or the photo-center of a binary) are done more than four times for one orbital period of the binary system.

For a close binary system with a short orbital period, we have a relatively large uncertainty in the position determination. For instance, the orbital period of Cyg-X1 is nearly 6 days, which are extremely shorter than that of normal binary stars, say a few months and

several years. Because of such an extreme condition, it is interesting to seek another method in addition to the standard one. Moreover, stars with planets also are another interesting target.

What can we do for orbit determination from position measurements with low signal-to-noise (SN) ratio? It is expected that the position of the object is measured many times. The dense region of the observed points is corresponding to the neighborhood of the apastron of the Kepler orbit, because the motion of the source star is slower according to the Kepler's second law. On the other hand, a region of fewer points is including the periastron, around which the source star moves faster. Therefore, a statistical analysis including the variance of the measured positions and their correlation will bring the information about the orbital elements of the binary system. Gedanken experiments suggest that the second moments are useful for exploring the shape of the orbit but they are not sufficient for the full orbit determination. At least the third moments seem to be needed. See Figs. 1 and 2.

Therefore, the main purpose of this paper is to propose a method for orbit determination of an astrometric binary with low SN ratio by using the second and third moments. We shall provide also an exact solution for the coupled equations. As a result, the orbital elements of the binary are written in terms of the second and third moments.

This paper is organized as follows. We present a formulation and the solution in § 2. In § 3, numerical tests are also done to see how reliable the analytic result is for practical cases taking account of observational noises. § 4 is devoted to Conclusion. Throughout this paper, the spatial coordinates are the angular positions normalized by the distance to the celestial object.

## 2. Basic Formulation

### 2.1. Motion in the orbital plane

Before projecting onto the celestial sphere, we consider a Kepler orbit, where the semi-major axis and semiminor one are denoted as  $a_K$  and  $b_K$ . We choose the  $(X, Y)$  coordinates on the orbital plane such that the  $X$ -axis is along the semimajor axis of the elliptic orbit, the  $Y$ -axis is along the semiminor one and the origin of the coordinates is chosen as the center of the ellipse. The orbit is expressed as

$$X = a_K \cos u, \tag{1}$$

$$Y = b_K \sin u, \tag{2}$$

where  $u$  denotes the eccentric anomaly.

By introducing the eccentricity  $e_K$ , the semiminor axis becomes

$$b_K = a_K \sqrt{1 - e_K^2}. \tag{3}$$

For an object in the Kepler motion, the time  $t$  is related with the position  $u$  through the so-called Kepler equation

$$t = t_0 + \frac{P}{2\pi}(u - e_K \sin u), \quad (4)$$

where  $t_0$  denotes the time of periastron passage. This equation represents transcendental equations in the sense that it cannot be solved analytically without any approximation. In other words,  $u$  cannot be expressed by using elementary functions of  $t$ . This makes the inverse problem in astrometry difficult.

## 2.2. Projection with respect to the line of sight

We assume a plane perpendicular to the line of sight, where this plane is safely considered a small part of the celestial sphere because the angular position shift of extra-solar objects is sufficiently small.

A reference frame, which is used in astrometric observations, is described by the  $(x, y)$  coordinates. As usual, the  $(X, Y)$  coordinates on the orbital plane and the  $(x, y)$  coordinates on the reference plane are related through

$$\begin{aligned} x &= (X - a_K e_k)(\cos \omega \cos \Omega - \sin \omega \sin \Omega \cos i) \\ &\quad - Y(\sin \omega \cos \Omega + \cos \omega \sin \Omega \cos i) \\ &= x_0 + \alpha \cos u + \beta \sin u, \end{aligned} \quad (5)$$

$$\begin{aligned} y &= (X - a_K e_k)(\cos \omega \sin \Omega + \sin \omega \cos \Omega \cos i) \\ &\quad - Y(\sin \omega \sin \Omega - \cos \omega \cos \Omega \cos i) \\ &= y_0 + \gamma \cos u + \delta \sin u, \end{aligned} \quad (6)$$

where  $x_0, y_0, \alpha, \beta, \gamma, \delta$  are defined as

$$x_0 \equiv -a_K e_K (\cos \omega \cos \Omega - \sin \omega \sin \Omega \cos i), \quad (7)$$

$$y_0 \equiv -a_K e_K (\cos \omega \sin \Omega + \sin \omega \cos \Omega \cos i), \quad (8)$$

$$\alpha \equiv a_K (\cos \omega \cos \Omega - \sin \omega \sin \Omega \cos i), \quad (9)$$

$$\beta \equiv -b_K (\sin \omega \cos \Omega + \cos \omega \sin \Omega \cos i), \quad (10)$$

$$\gamma \equiv a_K (\cos \omega \sin \Omega + \sin \omega \cos \Omega \cos i), \quad (11)$$

$$\delta \equiv -b_K (\sin \omega \sin \Omega - \cos \omega \cos \Omega \cos i). \quad (12)$$

Here,  $\Omega, \omega$  and  $i$  denote the longitude of ascending node, the argument of periastron and the inclination angle, respectively. See Fig. 3.

The ascending node and the descending one cannot be distinguished by astrometric observations alone. Therefore, both of  $\pm$  for  $i$  are possible. Furthermore, this paper focuses on the moments, so that the clockwise and anti-clockwise motions cannot be distinguished. Two pairs of  $(\Omega, \omega)$  are possible. Nevertheless, the shape of the orbit is uniquely determined as shown below.

### 2.3. Moment Formalism

Let us assume frequent observations of the angular position. Namely, we consider a large number of observed points. For such a case, the statistical average expressed as a summation is taken as the temporal average in an integral form as

$$\langle F \rangle \equiv \frac{1}{T_{obs}} \int_0^{T_{obs}} F dt, \quad (13)$$

where  $\langle \rangle$  denotes the mean and  $T_{obs}$  denotes the total time duration of the observations.

In this paper, we focus on the periodic motion, so that the above expression becomes the integration over one orbital period. We thus obtain

$$\begin{aligned} \langle F \rangle &= \frac{1}{P} \int_{t_0}^{t_0+P} F dt \\ &= \frac{1}{2\pi} \int_0^{2\pi} F(1 - e_K \cos u) du, \end{aligned} \quad (14)$$

where we used Eq. (4) and  $dt = (1 - e_K \cos u) du$ .

Let us consider statistical moments. Figure 1 suggests that the moments  $M_{xx}$  and  $M_{yy}$  are useful for distinguishing two different orbits. Next, we consider the periastron for the orbit denoted by the closed solid curve. For simplicity, we assume that it is located at positive  $x$  (in the right hand side of the ellipse). For this case, the object moves faster around the periastron and slower around the apastron. Hence, the dots in the figure schematically show asymmetry in the number of observed points. In order to distinguish such an asymmetry, the third moment such as  $M_{xxx}$  seems useful because of the odd parity. Figure 2 suggests that  $M_{xy}$  is needed via a Gedanken experiment. The second moments are defined as

$$\begin{aligned} M_{xx} &\equiv \langle (x - \langle x \rangle)^2 \rangle \\ &= \frac{1}{2}(\alpha^2 + \beta^2) - \frac{1}{4}e_K^2 \alpha^2, \end{aligned} \quad (15)$$

$$\begin{aligned} M_{yy} &\equiv \langle (y - \langle y \rangle)^2 \rangle \\ &= \frac{1}{2}(\gamma^2 + \delta^2) - \frac{1}{4}e_K^2 \gamma^2, \end{aligned} \quad (16)$$

$$\begin{aligned} M_{xy} &\equiv \langle (x - \langle x \rangle)(y - \langle y \rangle) \rangle \\ &= \frac{1}{2}(\alpha\gamma + \beta\delta) - \frac{1}{4}e_K^2 \alpha\gamma, \end{aligned} \quad (17)$$

The third moments are defined as

$$\begin{aligned} M_{xxx} &\equiv \langle (x - \langle x \rangle)^3 \rangle \\ &= \frac{3}{8}e_K \alpha(\alpha^2 + \beta^2) - \frac{1}{4}e_K^3 \alpha^3, \end{aligned} \quad (18)$$

$$\begin{aligned} M_{yyy} &\equiv \langle (y - \langle y \rangle)^3 \rangle \\ &= \frac{3}{8}e_K \gamma(\gamma^2 + \delta^2) - \frac{1}{4}e_K^3 \gamma^3, \end{aligned} \quad (19)$$

$$M_{xxy} \equiv \langle (x - \langle x \rangle)^2 (y - \langle y \rangle) \rangle$$

$$= \frac{1}{8}e_K(3\alpha^2\gamma + \beta^2\gamma + 2\alpha\beta\delta) - \frac{1}{4}e_K^3\alpha^2\gamma, \quad (20)$$

$$\begin{aligned} M_{xyy} &\equiv \langle (x - \langle x \rangle)(y - \langle y \rangle)^2 \rangle \\ &= \frac{1}{8}e_K(3\alpha\gamma^2 + \alpha\delta^2 + 2\beta\gamma\delta) - \frac{1}{4}e_K^3\alpha\gamma^2. \end{aligned} \quad (21)$$

The moments  $M_{xx}, \dots, M_{xyy}$  are actually observables.

The vanishing of all the third moments leads to  $e_K = 0$ . In the following, let us consider  $e_K \neq 0$  cases.

In the above second and third moments, the specific combinations among  $\alpha, \beta, \gamma, \delta$  frequently appear. Therefore, it is convenient to define new variables as

$$I_1 \equiv \alpha^2 + \beta^2, \quad (22)$$

$$I_2 \equiv \gamma^2 + \delta^2, \quad (23)$$

$$I_3 \equiv \alpha\gamma + \beta\delta. \quad (24)$$

By using the moments expressed by Eqs. (15)-(17), the variables  $I_1, I_2, I_3$  are rewritten as

$$I_1 = \frac{1}{2}e_K^2\alpha^2 + 2M_{xx}, \quad (25)$$

$$I_2 = \frac{1}{2}e_K^2\gamma^2 + 2M_{yy}, \quad (26)$$

$$I_3 = \frac{1}{2}e_K^2\alpha\gamma + 2M_{xy}. \quad (27)$$

Eq. (25) is substituted into Eq. (18) to obtain a cubic equation for  $e_K\alpha$  as

$$(e_K\alpha)^3 - 12M_{xx}(e_K\alpha) + 16M_{xxx} = 0. \quad (28)$$

This cubic equation gives three roots as  $e_K\alpha$  by using Cardano's formula. For saving the space, we do not write down the formula. In the similar manner, we obtain from Eqs. (26) and (19)

$$(e_K\gamma)^3 - 12M_{yy}(e_K\gamma) + 16M_{yyy} = 0. \quad (29)$$

This provides  $e_K\gamma$ , where its multiplicity is three.

At this point, we know both  $e_K\alpha$  and  $e_K\gamma$ , which can be substituted into Eqs. (25)-(27). We thus obtain the value of the variables  $I_1, I_2$  and  $I_3$ .

In general, we get multi values for  $e_K\alpha$  and  $e_K\gamma$ . However, they are true solutions for Eqs. (28) and (29), whereas not all of them satisfy the observed third moments. They have to satisfy the remaining set of the third moments as

$$M_{xxy} = \frac{1}{8}(e_K\gamma)I_1 + \frac{1}{4}(e_K\alpha)I_3 - \frac{1}{4}(e_K\alpha)^2(e_K\gamma), \quad (30)$$

$$M_{xyy} = \frac{1}{8}(e_K\alpha)I_2 + \frac{1}{4}(e_K\gamma)I_3 - \frac{1}{4}(e_K\alpha)(e_K\gamma)^2, \quad (31)$$

which can be used to pick up the correct  $e_K\alpha$  and  $e_K\gamma$  from multiple candidate values.

The definition of  $I_1$  by Eq. (22) is rewritten as

$$\alpha^2 = -\beta^2 + I_1, \quad (32)$$

which tells us  $\alpha$  as a function of  $\beta$

$$\alpha = \pm\sqrt{-\beta^2 + I_1}. \quad (33)$$

It is obvious that the sign of the right hand side of Eq. (33) must be the same as that of the left hand side, namely  $\alpha$ . For  $e_K \neq 0$ , the sign of  $\alpha$  is the same as that of  $e_K\alpha$  that has been obtained above. This is expressed by

$$\text{sgn}(\alpha) = \text{sgn}(e_K\alpha), \quad (34)$$

where  $\text{sgn}$  denotes the sign. Therefore, the sign of the right hand side of Eq. (33) is obtained uniquely as  $\text{sgn}(e_K\alpha)$ . Eq. (33) thus becomes

$$\alpha = \text{sgn}(e_K\alpha)\sqrt{-\beta^2 + I_1}. \quad (35)$$

What is the difference between Eqs. (33) and (35)? Eq. (33) means two different equations because of  $\pm$  in the right hand side, whereas Eq. (35) is a *single* one.

For the later convenience, we define  $\Gamma$  as

$$\Gamma \equiv \frac{\gamma}{\alpha}, \quad (36)$$

which is obtained from known quantities  $e_K\alpha$  and  $e_K\gamma$  as  $\Gamma = (e_K\gamma)(e_K\alpha)^{-1}$ .

We substitute Eq. (36) into the definition of  $I_3$  by Eq. (24) in order to delete  $\gamma$ . We obtain

$$\alpha^2 = \frac{I_3 - \beta\delta}{\Gamma}. \quad (37)$$

This is substituted into the definition of  $I_1$  by Eq. (22). We obtain

$$\delta = \frac{\beta^2\Gamma + I_3 - I_1\Gamma}{\beta}. \quad (38)$$

This is a function of only  $\beta$ .

Eqs. (36) and (38) are substituted into  $\gamma$  and  $\delta$  in Eq. (23). After rather lengthy calculations, we get

$$\beta^2 = \frac{(I_3 - I_1\Gamma)^2}{I_1\Gamma^2 + I_2 - 2I_3\Gamma}, \quad (39)$$

where we used Eq. (22) for  $\alpha^2$ . Interestingly, the right hand side of this equation consists of only the known quantities  $I_1$ ,  $I_2$ ,  $I_3$  and  $\Gamma$ . Therefore, we obtain the value of  $\beta^2$ , which determines  $\alpha$  through Eq. (35).

Eq. (39) is solved for  $\beta$  as

$$\beta = \pm \frac{I_3 - I_1\Gamma}{\sqrt{I_1\Gamma^2 + I_2 - 2I_3\Gamma}}. \quad (40)$$

Unfortunately, we do not know  $e_K\beta$  contrary to  $e_K\alpha$ . Therefore, the sign of the right hand side of Eq. (40) is not uniquely determined. The multiplicity of  $\beta$  is two and hence that of  $\delta$  is also two according to Eq. (38).

Up to this point, we know the value of  $\alpha$  and  $e_K\alpha$  from observed quantities. We thus find separately  $e_K$  as  $e_K = (e_K\alpha)\alpha^{-1}$ . It is crucial in the following procedure that the eccentricity  $e_K$  is determined at this step.

It is very inconvenient that  $\beta$  and  $\delta$  are proportional to the semiminor axis  $b_K$  in their definition. We know  $e_K$ , so that  $b_K$  can be expressed by  $a_K$ . Hence, we define renormalized quantities as

$$\begin{aligned}\tilde{\beta} &\equiv \frac{\beta}{\sqrt{1-e_K^2}} \\ &= -a_K(\sin\omega\cos\Omega + \cos\omega\sin\Omega\cos i),\end{aligned}\tag{41}$$

$$\begin{aligned}\tilde{\delta} &\equiv \frac{\delta}{\sqrt{1-e_K^2}} \\ &= -a_K(\sin\omega\sin\Omega - \cos\omega\cos\Omega\cos i),\end{aligned}\tag{42}$$

where we used Eqs. (10) and (12). We know the values of  $\beta$ ,  $\delta$  and  $e_K$ . Therefore, one can estimate  $\tilde{\beta}$  and  $\tilde{\delta}$ .

One can construct from four variables  $\alpha$ ,  $\tilde{\beta}$ ,  $\gamma$ ,  $\tilde{\delta}$ , some quantities that are dependent on the inclination angle  $i$  but not on any other angles  $\omega$  nor  $\Omega$ . One example is

$$\begin{aligned}C &\equiv \alpha^2 + \tilde{\beta}^2 + \gamma^2 + \tilde{\delta}^2 \\ &= a_K^2(1 + \cos^2 i).\end{aligned}\tag{43}$$

Another is

$$\begin{aligned}D &\equiv \alpha\tilde{\delta} - \tilde{\beta}\gamma \\ &= a_K^2\cos i.\end{aligned}\tag{44}$$

These relations can be verified by direct calculations. Note that  $D$  must be positive because  $\cos i \geq 0$ . This positivity chooses one pair of  $(\tilde{\beta}, \tilde{\delta})$  and reject the other pair. Only the pair of  $(\beta, \delta)$  is thus obtained. We know  $\alpha$ ,  $\gamma$ ,  $\tilde{\beta}$ ,  $\tilde{\delta}$ , so that  $C$  and  $D$  can be estimated.

By deleting  $a_K^2$  from Eqs. (43) and (44), we obtain

$$\cos^2 i - \frac{C}{D}\cos i + 1 = 0.\tag{45}$$

This is a quadratic equation for  $\cos i$ . Apparently, two cases of  $\cos i$  are possible. However, this is not the case. By using Newton's identities for Eq. (45), we obtain the identity as

$$(\cos i_1) \times (\cos i_2) = 1,\tag{46}$$

where  $\cos i_1$  and  $\cos i_2$  denote the two roots for Eq. (45). The inequality as

$$|\cos i| \leq 1,\tag{47}$$

thus leads to the unique value of  $\cos i$ , because the other exceeds the unity as its absolute value.

The single value of  $\cos i$  provides positive  $i$  and negative one. They are corresponding to the ascending node and the descending node, respectively. They cannot be distinguished by

astrometric observations alone. In order to distinguish them, radial velocity measurements for instance are needed.

We get the value of the inclination angle. From Eq. (44), therefore, the semimajor axis is obtained as

$$a_K = \sqrt{\frac{D}{\cos i}}. \quad (48)$$

This suggests that the value of  $a_K$  is uniquely determined but not doubly.

In order to determine  $\omega$  and  $\Omega$ , let us consider other combinations among  $\alpha, \gamma, \tilde{\beta}, \tilde{\delta}$ .

Direct calculations lead to

$$\alpha^2 + \tilde{\beta}^2 = a_K^2 (\cos^2 \Omega + \sin^2 \Omega \cos^2 i), \quad (49)$$

$$\gamma^2 + \tilde{\delta}^2 = a_K^2 (\sin^2 \Omega + \cos^2 \Omega \cos^2 i). \quad (50)$$

The ratio of them is denoted as

$$\begin{aligned} r_1 &\equiv \frac{\gamma^2 + \tilde{\delta}^2}{\alpha^2 + \tilde{\beta}^2} \\ &= \frac{\sin^2 \Omega + \cos^2 \Omega \cos^2 i}{\cos^2 \Omega + \sin^2 \Omega \cos^2 i}. \end{aligned} \quad (51)$$

This is solved for  $\Omega$  as

$$\tan^2 \Omega = \frac{r_1 - \cos^2 i}{1 - r_1 \cos^2 i}, \quad (52)$$

which gives the values of  $\Omega$  because we have already determined  $i$  and  $r_1$ . As mentioned already, both of  $\pm\Omega$  are allowed.

Next, we consider different combinations as

$$\alpha^2 + \gamma^2 = a_K^2 (\cos^2 \omega + \sin^2 \omega \cos^2 i), \quad (53)$$

$$\tilde{\beta}^2 + \tilde{\delta}^2 = a_K^2 (\sin^2 \omega + \cos^2 \omega \cos^2 i), \quad (54)$$

which can be verified by direct calculations. The ratio of them is denoted as

$$\begin{aligned} r_2 &\equiv \frac{\tilde{\beta}^2 + \tilde{\delta}^2}{\alpha^2 + \gamma^2} \\ &= \frac{\sin^2 \omega + \cos^2 \omega \cos^2 i}{\cos^2 \omega + \sin^2 \omega \cos^2 i}. \end{aligned} \quad (55)$$

This is solved for  $\omega$  as

$$\tan^2 \omega = \frac{r_2 - \cos^2 i}{1 - r_2 \cos^2 i}, \quad (56)$$

which tells us the values of  $\omega$  because we have already determined  $i$  and  $r_2$ . As mentioned already, both of  $\pm\omega$  are possible.

At most four values of  $\Omega$  are possible. Similarly, the maximum multiplicity of  $\omega$  is four. In total, sixteen sets of  $(\omega, \Omega)$  appear to exist. The multiplicity of  $(\omega, \Omega)$  is reduced, because they must satisfy the definition of  $\alpha, \beta, \gamma, \delta$  with the uniquely determined  $a_K, e_K$  and  $\cos i$ .



In particular,  $\alpha, \beta, \gamma, \delta$  include different combinations of sin and cos. Basically, the sign of sin and cos has four types  $(+, +), (+, -), (-, +), (-, -)$ . Hence, the apparent multiplicity sixteen is divided by four. In addition, it is obvious from Eqs. (9)-(12) that the sign of  $\Omega$  depends on that of  $\omega$ . The multiplicity is thus divided also by two. As a consequence, we get only the two pairs of  $(\Omega, \omega)$ . One pair is corresponding to the clockwise motion and the other to the anti-clockwise one.

### 3. Discussion

#### 3.1. Numerical test

The above formalism is discussed in an idealized world. Numerical tests are done below to see whether the analytic result works for practical cases. First, Eqs. (13) and (14) assume that one can integrate observed quantities. In practice, however, observations are discrete, for which the integration becomes a summation. The integration and the summation could agree in the limit that the number of observations  $N$  approaches the infinity. In a real world,  $N$  is a large number but much smaller than the infinity. Does the above formalism still give a reliable answer? For investigating this point, we perform numerical simulations. According to the simulation for observations with equal time interval, the above formalism recovers perfectly the orbital parameters for  $N = 100$ .

Next, we consider observation noises. The above formalism assumes that the observed points are located on an apparent ellipse. However, position measurements are inevitably associated with observational errors. Therefore, we perform numerical simulations by adding Gaussian errors into the position measurements as  $x \rightarrow x + \Delta x$  and  $y \rightarrow y + \Delta y$ , where  $\Delta x$  and  $\Delta y$  obey Gaussian distributions with the standard deviation  $\sigma$ . We consider two cases:  $\sigma = 0.1$  (smaller case) and  $0.5$  (larger one) in the units of  $a_K = 1$ . Table 1 is a list of the orbital parameters that are recovered by using the above formalism. See Fig. 5 for simulated points in a  $N = 100$  simulation for  $\sigma = 0.1$  and  $0.5$ . For small observation error cases, the orbital parameters are well recovered. For large observation errors comparable to a half of the semimajor axis, however, the recovered angles  $i, \omega$  and  $\Omega$  are far from the true ones. On the other hand, the eccentricity  $e_K$  and the semimajor axis  $a_K$  are recovered better than the angles. The semimajor axis is overestimated, because the simulated second moments apparently become larger than the true ones owing to such a large dispersion. We numerically study also different parameter values. They lead to similar results, for which numerical tables are omitted for saving the space.

Our numerical tests for the discreteness of observations and for the observation noises suggest that the above formalism derived for the idealized system could work in practice if observation noises are not so large.

The previous analytical method cannot guess orbit parameters for such large measure-

ment errors  $\sigma = 0.5$ , mostly because  $\cos i$  apparently becomes larger than the unity (namely, the data points fit better with open orbits) (Asada et al. 2007).

Up to this point, we have assumed that the orbital period is known. What happens for unknown binaries? We have made Fourier analyses for numerically simulated points with time in Fig. 5. In the time domain, the Fourier spectrum has two peaks. One peak corresponds to the orbital period and the other is around the artificial time step in the numerical simulations. This suggests that the moment approach can be applied also to unknown binary systems, if a Fourier analysis is adequately used to know the orbital period. Namely, the present method could be used to search new binary systems.

Let us consider Cyg-X1,  $a \sim 0.2$  AU at 2 kpc from us. The expected angular accuracy in JASMINE is  $\sim 10$  microarcsec, so that the semimajor axis of Cyg-X1 can become a direct observable. Other known X-ray binaries seem too faint to be observed by JASMINE.

A Sun-like star at 20 pc with Jupiter-like planet at 1 AU could produce a wobble of 0.001 AU, corresponding to 50 microarcsec., which must be an interesting target.

### 3.2. Proper motion of the binary

In the main part of this paper, we ignore the proper motion of the binary system in our galaxy. This is mostly because, for a close binary, the proper motion of the binary in our galaxy causes a larger cumulative displacement than the orbital motion of the component stars, though the orbital velocity may be larger than the proper motion. In advance, therefore, we know the proper motion before determining the orbital elements. For instance, it can be done by a comparison between the Hipparcos data and the future space astrometry. If one wishes to determine the proper motion  $(v_x, v_y)$  in the present formalism, however, the apparent positions should be replaced as  $x \rightarrow x + v_x t$  and  $y \rightarrow y + v_y t$ . By averaging the observed position according to Eq. (13), we obtain

$$\begin{aligned} \langle x \rangle &= \frac{1}{2} T_{obs} v_x + const. + O\left(\frac{T_K}{T_{obs}} a_K\right), \\ \langle y \rangle &= \frac{1}{2} T_{obs} v_y + const. + O\left(\frac{T_K}{T_{obs}} a_K\right), \end{aligned} \quad (57)$$

where the terms of  $O(a_K T_K T_{obs}^{-1})$  in the right hand side come from the Kepler motion. Hence the terms are nothing but a decaying term such as  $T_{obs}^{-1} \cos u_{obs}$  for the eccentric anomaly  $u_{obs}$  corresponding to  $t = T_{obs}$ . They become negligible as  $T_{obs} T_K^{-1} \rightarrow \infty$ . Furthermore, the cumulative translation by the proper motion exceeds the oscillatory displacement by the Kepler motion for a close binary. That is,  $a_K (T_{obs} v)^{-1} \ll 1$ , where  $v \equiv \sqrt{v_x^2 + v_y^2}$ . Owing to this effect, the decaying part due to the Kepler motion goes away for a long observation period  $T_{obs}$ , say  $> 1$  yr.

The parts growing linearly in the observation time  $T_{obs}$  give the information about  $(v_x, v_y)$ , provided  $T_{obs}$  is taken as a variable in the data analysis. If  $T_{obs} \gg T_K$ , the above extraction of the linearly growing part will be possible, especially for a short-separation binary.

### 3.3. Mildly relativistic compact binary

Finally, we mention a mildly relativistic compact binary, in which the relativistic advance of the periastron occurs. Rigorously speaking, we have to take account of the general relativistic equations. In practice, however, the above method may be applied. For instance, let us imagine two-year observations. For the first-year data, the periastron direction  $\varpi_1$  is derived. The second-year data tells  $\varpi_2$ . The difference between the first-year and second-year directions of the periastron suggests the periastron advance as  $(\varpi_2 - \varpi_1)\text{yr}^{-1}$ .

For instance, the Hulse-Taylor binary pulsar shows the large periastron shift rate  $\dot{\varpi} = 4$  deg. per year, though the angular orbital radius is a few microarcsec. and it is beyond the current measurement capability.

## 4. Conclusion

This paper proposed a moment approach for orbit determinations of a close binary system with a short orbital period from astrometric observations alone. As an exact solution to the coupled equations, the orbital elements are written in terms of the second and third moments of the projected position that is measured by astrometry.

The moment formalism does not replace the standard method using Kepler equation. It is safer to say that the present formalism is a supplementary tool for giving a rough parameter estimation, which can be used as a trial value for full numerical data fittings. It is interesting to make numerical tests of the present method. It is left as a future work.

In the moment approach, the temporal information is smeared. Therefore, the orbital period cannot be determined by this method. Another method such as the Fourier analysis of position data with time (in Fig. 5 for example) would give a characteristic frequency that is the inverse of the orbital period. Fourier analyses recover the orbital period from numerically simulated data for Fig. 5. This suggests that the moment approach can be applied also to unknown binary systems, if a Fourier analysis is adequately used to know the orbital period. Namely, the method could be used to search new binary systems.

We would like to thank Professor N. Gouda for useful information on astrometry missions. We wish to thank the JASMINE science WG member for stimulating conversations. We would be grateful to Y. Sendouda, R. Takahashi and K. Izumi for helpful conversations on numerical simulations. This work was supported in part (H.A.) by a Japanese Grant-in-Aid for Scientific Research from the Ministry of Education, No. 21540252 (Kiban-C) and in part (K.Y.) by JSPS research fellowship for young scientists.

## References

- Aitken, R. G. 1964 *The Binary Stars* (NY: Dover)
- Asada, H., Akasaka, T., & Kasai, M. 2004, PASJ, 56, L35

- Asada, H. Akasaka, T., & Kudoh, K. 2007, *AJ*, 133, 1243.
- Asada, H. 2008, *PASJ*, 60, 843
- Binnendijk, L. 1960 *Properties of Double Stars* (Philadelphia: University of Pennsylvania Press).
- Catovic, Z., & Olevic, D. 1992 in *IAU Colloquium 135, ASP Conference Series Vol. 32* (eds McAlister H. A., Hartkopf W. I., ) 217-219 (San Francisco, Astronomical Society of the Pacific).
- Danby, J. M. A., 1988 *Fundamentals of Celestial Mechanics* (VA: William-Bell)
- Eichhorn, H. K., & Xu, Y. 1990, *ApJ*, 358, 575
- Gouda, N. et al. 2007, *Advances in Space Research*, 40, 664.
- Mignard, F. ‘Overall Science Goals of the Gaia Mission’, *Proc. The Three-Dimensional Universe with Gaia*, 4-7 October 2004, Paris (Netherlands: ESA Publications)
- Olevic, D., & Cvetkovic, Z. 2004, *A&A*, 415, 259
- Perryman, M. A. C. ‘Overview of the Gaia Mission’, *Proc. The Three-Dimensional Universe with Gaia*, 4-7 October 2004, Paris (Netherlands: ESA Publications)
- Roy, A. E. 1988 *Orbital Motion* (Bristol: Institute of Physics Publishing)
- Thiele, T. N. 1883, *Astron. Nachr.*, 104, 245

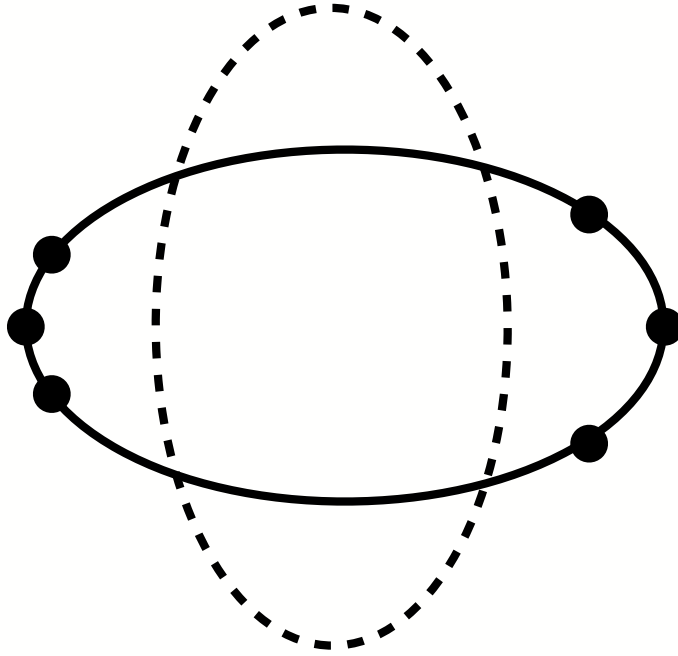


**Fig. 1.** Comparison between the second moments  $M_{xx}$  and  $M_{yy}$ . The orbit denoted by the closed solid curve has a larger variance along the  $x$ -axis, where  $M_{xx}$  is larger than  $M_{yy}$ . On the other hand, for the orbit denoted by the closed dashed curve,  $y$  components of the position have a larger scatter, where  $M_{yy}$  is larger than  $M_{xx}$ .

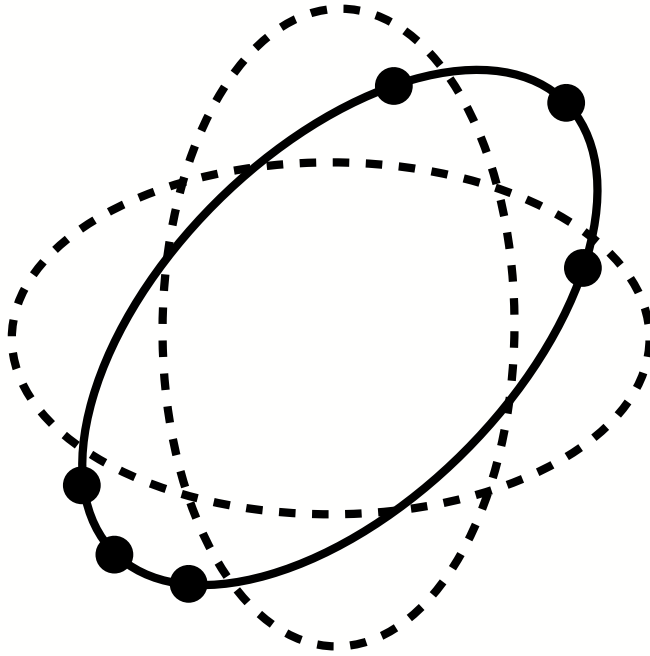


**Fig. 2.** Dashed curves denote two orbits: One is the semimajor axis along the  $x$ -axis. The other is along the  $y$ -axis. The orbit denoted by the solid curve is not distinguished by using the second moments  $M_{xx}$  and  $M_{yy}$ . The moment  $M_{xy}$  is thus needed.

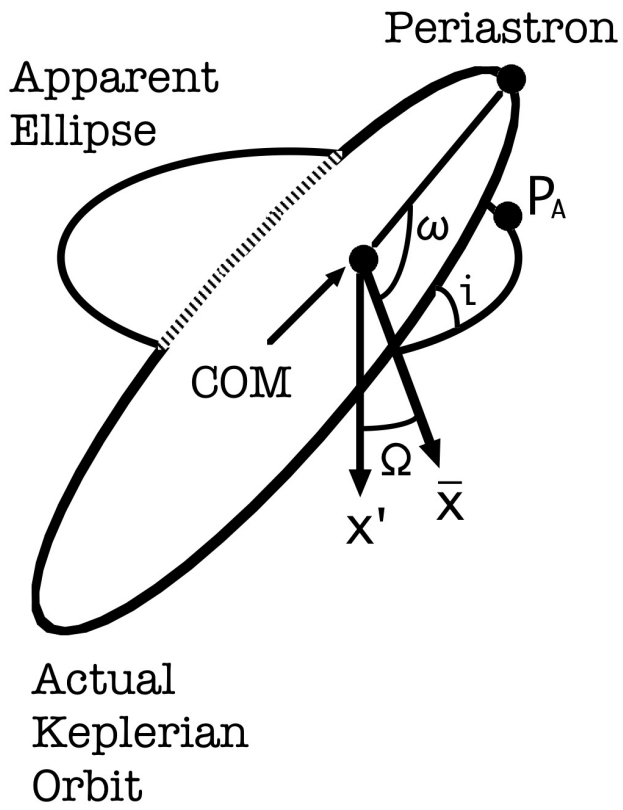


**Fig. 3.** Actual Keplerian orbit and apparent ellipse in three-dimensional space. We denote the inclination angle as  $i$ , the argument of periastron as  $\omega$  and the longitude of ascending node as  $\Omega$ . These angles relate two coordinates  $(x', y')$  and  $(\bar{x}, \bar{y})$ , both of which choose the origin as the common center of mass. Here, the  $x'$  axis is taken to lie along the semimajor axis of the apparent ellipse, while the  $\bar{x}$ -axis is along the direction of the ascending node.

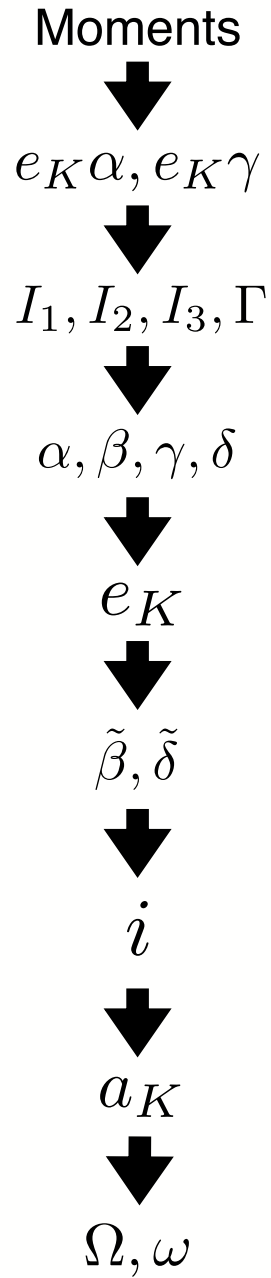


**Fig. 4.** Flowchart of parameter determinations in the moment formalism. The starting point is evaluating the moments from astrometric observations.



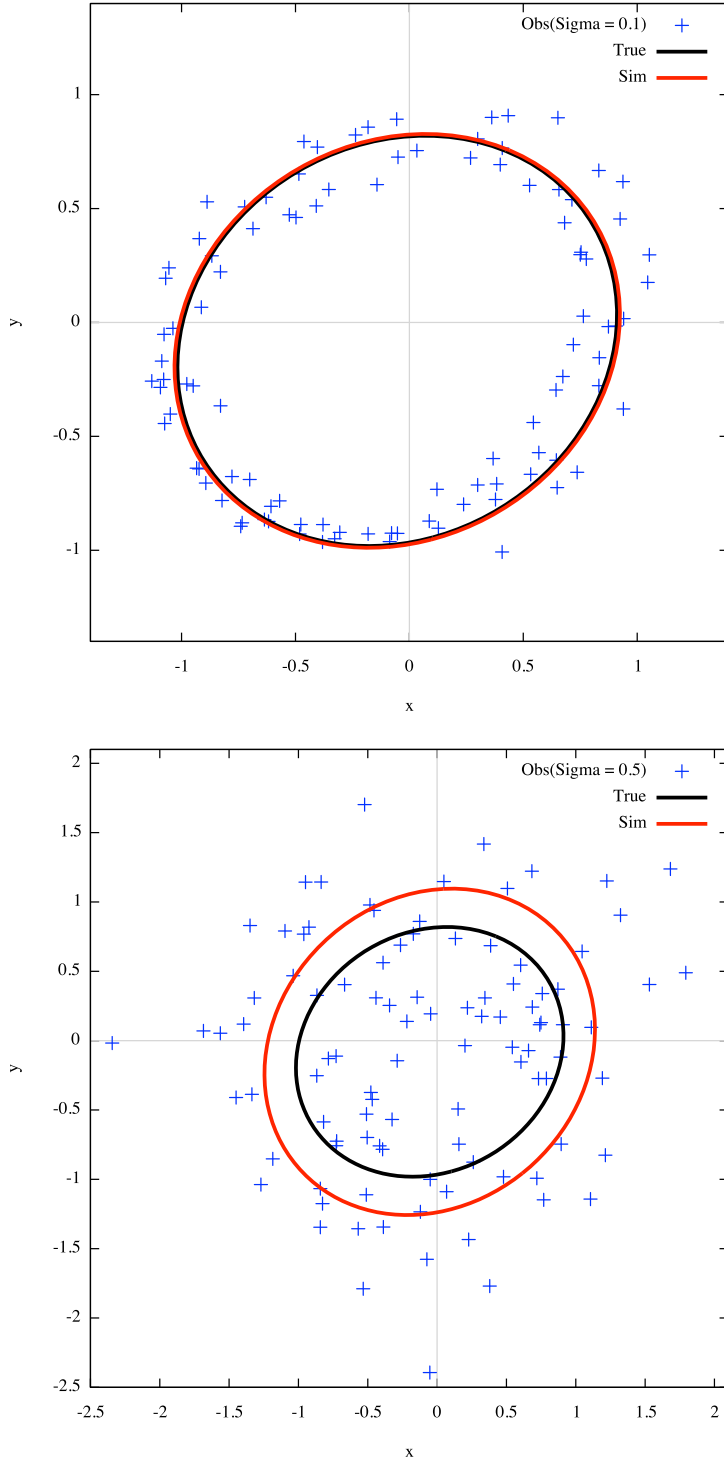


**Fig. 5.** One hundred observed points of the same source star in the  $x - y$  plane for a simulation with constant time interval. The parameters are  $\omega = 30$  [deg.],  $\Omega = 30$  [deg.],  $i = 30$  [deg.],  $e_K = 0.1$ ,  $a_K = 1.0$  and  $N = 100$ . The black curve and the gray (red in color) one denote orbits for the true parameter and for the mean value of the recovered parameters, respectively. Top: Gaussian errors  $\sigma = 0.1$ . Bottom:  $\sigma = 0.5$ .

**Table 1.** Reconstructing the parameters for numerical simulations for three different eccentricity cases as  $e_K = 0.1, 0.3, 0.5$ . In the table, the row  $\sigma = 0$  indicates true orbital parameters, whereas the rows  $\sigma = 0.1$  and  $0.5$  provide the recovered values for adding Gaussian errors (0.1 or 0.5 in the units of the true semimajor axis, respectively). For each parameter set, 100 runs are done and the mean and the standard deviation are also evaluated.

$\sigma$	$e_k$	$a_k$	$i$ [deg.]	$\omega$ [deg.]	$\Omega$ [deg.]
0	0.1	1.0	30.0	30.0	30.0
0.1	$0.09454 \pm 0.02518$	$1.011 \pm 0.01423$	$30.02 \pm 2.039$	$22.37 \pm 17.45$	$29.81 \pm 4.205$
0.5	$0.1445 \pm 0.09343$	$1.257 \pm 0.07624$	$28.87 \pm 7.731$	$43.87 \pm 25.79$	$40.75 \pm 22.62$
0	0.3	1.0	30.0	30.0	30.0
0.1	$0.2936 \pm 0.02269$	$1.011 \pm 0.01526$	$30.04 \pm 2.228$	$28.73 \pm 8.557$	$30.20 \pm 4.687$
0.5	$0.2327 \pm 0.1211$	$1.266 \pm 0.08215$	$29.63 \pm 7.189$	$41.26 \pm 25.13$	$35.45 \pm 18.14$
0	0.5	1.0	30.0	30.0	30.0
0.1	$0.4793 \pm 0.03103$	$1.005 \pm 0.02253$	$30.34 \pm 2.477$	$27.53 \pm 8.234$	$31.72 \pm 5.709$
0.5	$0.3065 \pm 0.1223$	$1.233 \pm 0.07314$	$31.33 \pm 5.519$	$39.78 \pm 26.46$	$40.78 \pm 16.08$